SCIENTIFIC REPORTS
nature research

OPEN

The improvement of photocatalysis O_2 production over $BiVO_4$ with amorphous FeOOH shell modification

Ying Zhang, Lei Shi*, Zhongxing Geng, Tieqiang Ren & Zhanxu Yang*

A novel amorphous FeOOH modified $BiVO_4$ photocatalyst (A-FeOOH/$BiVO_4$) was successfully produced and characterized by various techniques. The results showed that amorphous FeOOH with about 2 nm thickness evenly covered on $BiVO_4$ surface, which caused resultant A-FeOOH/$BiVO_4$ exhibiting higher visible light photocatalytic performance for producing O_2 from water than $BiVO_4$. When the covered amount of amorphous FeOOH was 8%, the resultant photocatalyst possessed the best photocatalytic performance. To find the reasons for the improvement of photocatalytic property, electrochemical experiments, DRS, PL and BET, were also measured, the experimental results indicated that interface effect between amorphous FeOOH and $BiVO_4$ could conduce to migration of photogenerated charge, and exhibit stronger light responded capacity. These positive factors promoted A-FeOOH/$BiVO_4$ presenting improved the photocatalytic performance. In a word, the combination of amorphous FeOOH with $BiVO_4$ is an effective strategy to conquer important challenges in photocatalysis field.

Semiconductor photocatalysis has achieved keen attention in utilizing solar power to solve environments deterioration and energy crisis[1–3]. Hence, numerous photocatalyst materials were developed, including TiO_2[4–6], ZnO[7], WO_3[8–10], CdS[11,12], SnS_2[13], Ag based photocatalysts[14–16], etc. However, the development of photocatalysts with high efficient is still a huge and continuous undertaking.

The Bi-based photocatalyst materials, such as Bi_2O_3[17], BiOCl[18], BiOBr[19], BiOI[20], $BiVO_4$[21–23], Bi_2WO_6[24], and Bi_2MoO_6[25], have obtained great attention. Among these as-prepared photocatalysts, $BiVO_4$ with strong visible light response capacity and good stability has been extensively investigated in environmental remediation and water splitting[26–31]. Nevertheless, a big problem that affects the photocatalytic property of $BiVO_4$ is its unsatisfied charge carrier separated efficiency. To conquer this problem, many researchers had developed some methods for modifying $BiVO_4$. Cao *et al.* successfully prepared Au-$BiVO_4$ photocatalyst, which could present much higher visible-light photocatalytic performance for wastewater treatment and clean energy product than the individual $BiVO_4$[32]. Except Au modification, Pd, AuPd and CoPd were used to modify $BiVO_4$ to enhance its photocatalytic property[33–35]. However, these noble metals or noble metal alloys were high cost so that this method was difficult to be wide application. Hence, it was necessary to develop an economical and convenient method to modify $BiVO_4$.

Recently, amorphous semiconductor materials have been exploited and exhibited specific photocatalytic property[36,37]. Compared to crystals, amorphous semiconductor materials exist a most remarkable advantage that it possesses much smaller band gap than their crystalline counterparts, which conduces them to present more expansive light absorption range, which is an important condition for conversing solar energy[37]. However, amorphous semiconductor materials exhibited the short-range atomic order, and existed a number of defects, which could become the charge recombination centers, causing themselves inactive or weak performance. So could numerous defects existed on amorphous semiconductor materials as the electrons capturer be applied for modifying other photocatalysts? This view is very significative and interesting. Hence, considering the wide light responded property and cost, Fe based semiconductors enter into our view. Among Fe based semiconductors, FeOOH exhibits extensive visible light response capacity, which caused FeOOH coupled with other photocatalysts to modify the visible-light-irradiation photocatalytic property, some FeOOH with certain crystalline phase was used to modify photocatalyst materials, such as β-FeOOH/TiO_2[38], β-FeOOH/g-C_3N_4[39], α-FeOOH/$AgVO_3$[40],

College of Chemistry, Chemical Engineering and Environmental Engineering, Liaoning Shihua University, Fushun, 113001, China. *email: shilei_hit@qq.com; yangzhanxu@lnpu.edu.cn

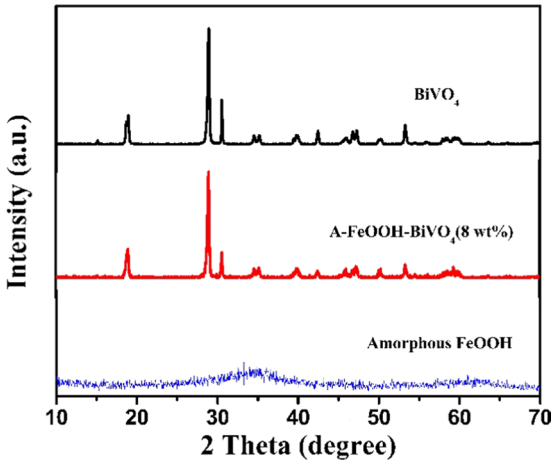

Figure 1. The X-ray diffraction patterns of as-prepared photocatalysts.

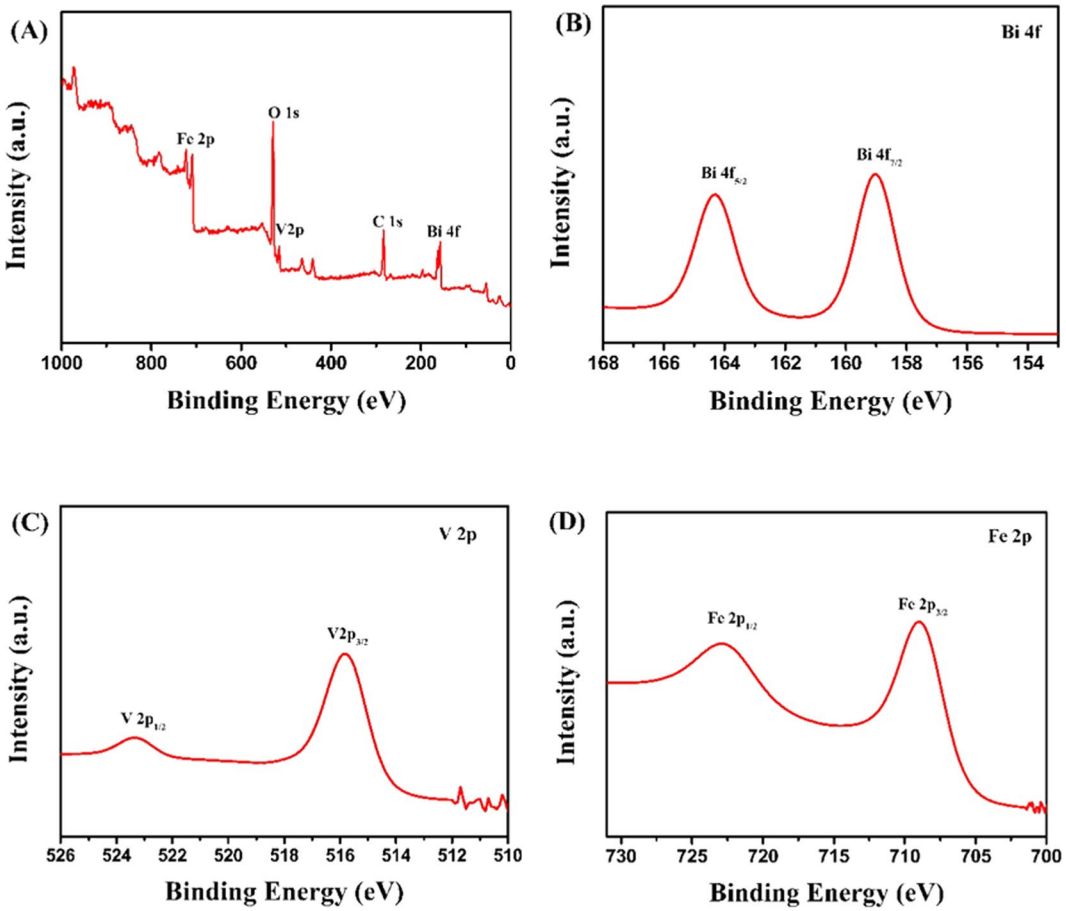

Figure 2. The XPS high resolution (**A**) survey spectra, (**B**) Bi 4f, (**C**) V 2p and (**D**) Fe 2p spectra of A-FeOOH/$BiVO_4$(8 wt%).

etc. Actually, FeOOH contained various crystalline phases, including α-phase, β-phase, δ-phase, γ-phase, and amorphous phase. Among these different crystalline phase FeOOH, amorphous FeOOH could exhibit excellent oxygen evolution rate by photoelectrochemical and superior pseudocapacitive performance[41,42]. However, it is relative lack of report about amorphous FeOOH as a modifier to be used in photocatalysis. Hence, combined with above proposed view, it is essential to investigate the role of amorphous FeOOH modifier.

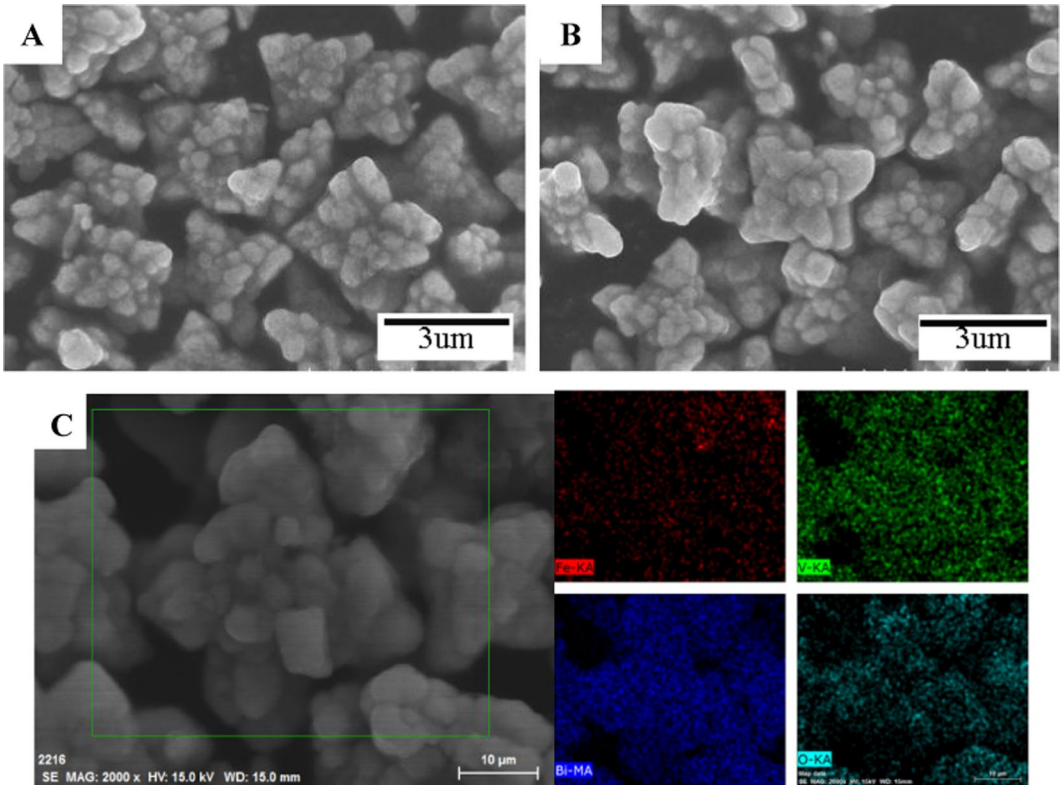

Figure 3. The SEM images of (**A**) $BiVO_4$ and (**B**) A-FeOOH/$BiVO_4$(8 wt%) and (**C**) SEM-EDS mapping images of A-FeOOH/$BiVO_4$(8 wt%).

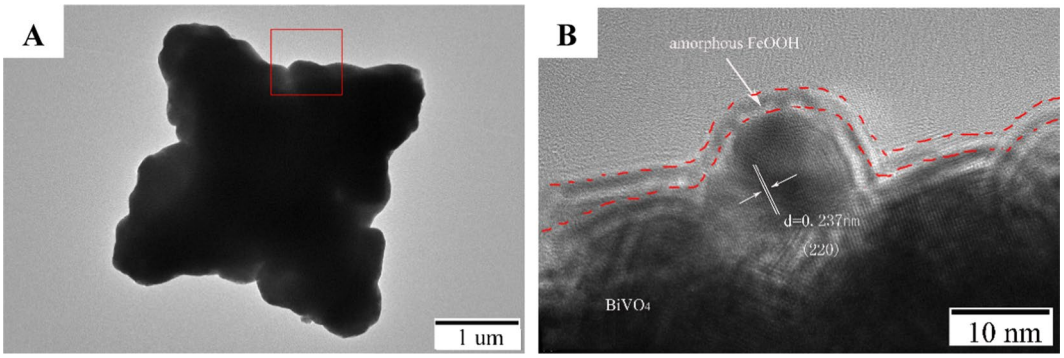

Figure 4. The (**A**) TEM and (**B**) HRTEM images of A-FeOOH/$BiVO_4$(8 wt%).

Herein, a novel amorphous FeOOH modified $BiVO_4$ was successfully prepared, and photocatalytic performance for producing O_2 from water was investigated. It could be found that, after amorphous FeOOH evenly covered the surface of $BiVO_4$, as-prepared photocatalysts exhibited better migration of photogenerated charges, and stronger visible light responded activity. These positive factors promoted A-FeOOH/$BiVO_4$ presenting improved the photocatalytic performance. Hence, this work shows an effective and simple modified method for designing and preparing highly efficient photocatalysis materials.

Experimental

The synthesis of catalysts. To obtain $BiVO_4$ material, in a beaker, $Bi(NO_3)_3{\cdot}5H_2O$ (5 mmol) dissolved in HNO_3 solution (5 mL 3 mol·L^{-1}) and ethylene glycol (20 mL) mixed solution. Then in other beaker, NH_4VO_3 (5 mmol) and 0.25 g sodium dodecylbenzenesulfonate (SDBS) were dissolved in hot water (20 mL). After stirred for 30 min, above two solution mixed, and the pH of solution was adjusted to 5 using NaOH solution. Stirring for 60 min, obtained suspension solution was placed into high pressure reactor with PTFE liner, maintained at 180 °C for 24 h. After filtration, wash and desiccation, $BiVO_4$ was prepared.

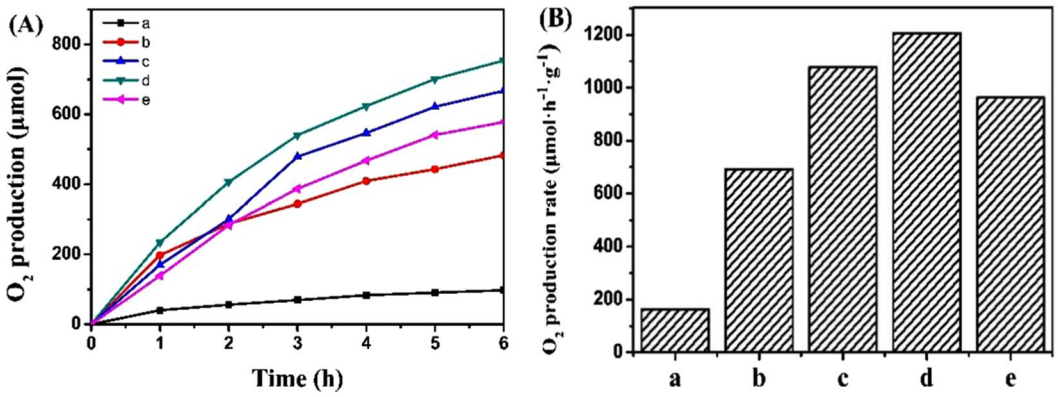

Figure 5. (**A**) Photocatalytic evolution O_2 curves and (**B**) OER over various samples, (a) $BiVO_4$, (b) A-FeOOH/$BiVO_4$(2 wt%), (c) A-FeOOH/$BiVO_4$(5 wt%), (d) A-FeOOH/$BiVO_4$(8 wt%) and (e) A-FeOOH/$BiVO_4$(10 wt%).

Samples	Light source	Application	Catalyst mass	Performance	References
WO_3	Visible light	O_2 production	200 mg	246.2 μmol in 5 h	[49]
$BiVO_4$ nano-leaves	Visible light	O_2 production	100 mg	300 μmol in 5 h	[50]
$BiVO_4$	Visible light	O_2 production	1000 mg	186 μmol in 6 h	[51]
a-Fe_2O_3	Visible light	O_2 production	10 mg	10.5 μmol in 15 h	[52]
A-FeOOH/$BiVO_4$(8 wt%)	Visible light	O_2 production	100 mg	723 μmol in 6 h	This work

Table 1. Comparison of photocatalytic activity in previous reports and this work.

Amorphous FeOOH/$BiVO_4$ was prepared as follows: $BiVO_4$ (400 mg) was mixed into 40 mL deionized water containing $FeCl_3{\cdot}6H_2O$ and NH_4HCO_3 (The molar ratio of $FeCl_3{\cdot}6H_2O$ and NH_4HCO_3 is 1:3). Stirring for 60 min, the solid powder was obtained through centrifugation, wash and desiccation. According to the theoretical content of amorphous FeOOH in amorphous FeOOH/$BiVO_4$, the obtained powder catalysts were marked as A-FeOOH/$BiVO_4$(2 wt%), A-FeOOH/$BiVO_4$(5 wt%), A-FeOOH/$BiVO_4$(8 wt%) and A-FeOOH/$BiVO_4$(10 wt%), respectively.

Characterizations and photocatalytic experiment. Supporting Materials showed their details.

Results and Discussion

Figure 1 demonstrates the XRD of resultant photocatalysts. As can be observed, resultant $BiVO_4$ exhibited highly crystalline, and there were some mainly diffraction peaks at 2θ of 18.6°, 28.9°, 30.5°, 34.4°, 35.3°, 39.4°, 42.3°, 46.1°, 46.6°, 47.3°, 53.3°, 58.3° and 59.9°, which indexed (101), (013), (112), (200), (020), (211), (105), (123), (204), (024), (301), (303) and (224) diffraction planes of monoclinic $BiVO_4$[43]. For amorphous FeOOH, there was no obvious diffraction peak to be found. Hence, in A-FeOOH/$BiVO_4$(8 wt%), XRD diffraction peaks of $BiVO_4$ could only be detected. The XRD results exposed that amorphous FeOOH had little impact the crystal phase of $BiVO_4$. Moreover, no other diffraction peak was found, meaning that resultant samples possessed the high purity.

Whereafter, the XPS of A-FeOOH/$BiVO_4$(8 wt%) was further investigated. As revealed in Fig. 2A, Bi, V, O and Fe could be found in the survey XPS spectra, according with the composition of material. Bi 4 f XPS spectrum (Fig. 2B) presented 164.3 eV and 159.1 eV two peaks that attributed to Bi $4f_{5/2}$ and Bi $4f_{7/2}$ in $BiVO_4$[44,45]. V 2p XPS spectrum (Fig. 2C) had two peaks at 516.3 eV and 524.3 eV, matching with V $2p_{1/2}$ and V $2p_{3/2}$ in $BiVO_4$[46]. Figure 2D (Fe 2p XPS spectrum) shows 724.2 (Fe $2p_{1/2}$) and 710.8 eV (Fe $2p_{3/2}$) that were consistent with FeOOH[47]. Hence, the results of XPS further confirmed that sample contained FeOOH and $BiVO_4$, consistent to the XRD.

The morphologies of $BiVO_4$ and A-FeOOH/$BiVO_4$(8 wt%) were seen through SEM. As revealed in Fig. 3, $BiVO_4$ and A-FeOOH/$BiVO_4$(8 wt%) exhibited similar star-shaped particles with the size of about 3.5 μm, which demonstrated that introduced amorphous FeOOH did not influence on the feature of $BiVO_4$. In addition, the elemental compositions of the resultant A-FeOOH/$BiVO_4$(8 wt%) were measured through EDS mapping analysis. The related element mapping images were exhibited in Fig. 3C. Clearly, Fe, V, Bi and O only appeared in observed view, meaning the successful preparation of A-FeOOH/$BiVO_4$.

Subsequently, to further observe the microstructure of A-FeOOH/$BiVO_4$, transmission electron microscopy were also analyzed. As revealed in Fig. 4A, A-FeOOH/$BiVO_4$(8 wt%) exhibited the similar star-shaped particles, which was consistent with the SEM. Clearly, amorphous FeOOH could not be observed at low resolution TEM image. As a result, the HRTEM of A-FeOOH/$BiVO_4$ (Fig. 4B) was provided. The lattice fringe spacing of 0.237 nm attributed to $BiVO_4$ (220) was obviously observed. Moreover, the thickness of ultrathin amorphous FeOOH nanolayers was about 2 nm, and evenly adhered on the surface of $BiVO_4$. Amorphous FeOOH nanolayers did not reveal a lattice spacing, demonstrating traditional amorphous structure.

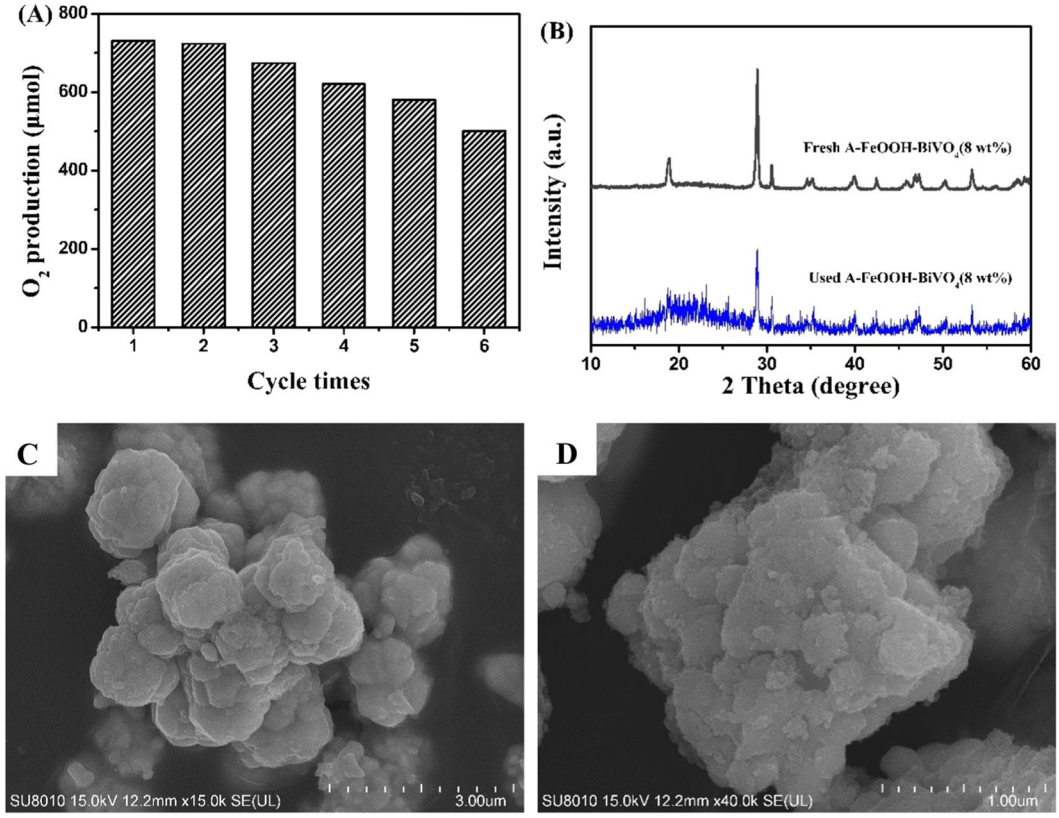

Figure 6. (**A**) Stability test in O_2 photosynthesis for A-FeOOH/$BiVO_4$(8 wt%), (**B**) the XRD of fresh A-FeOOH/$BiVO_4$(8 wt%) and used A-FeOOH/$BiVO_4$(8 wt%) and (**C,D**) The SEM images of used A-FeOOH/$BiVO_4$(8 wt%).

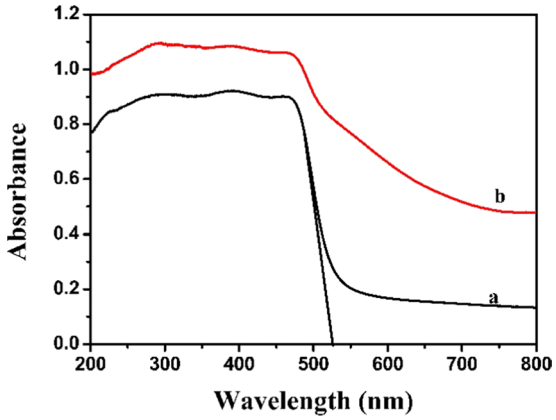

Figure 7. The UV-Vis absorption spectrum of (**a**) $BiVO_4$ and (**b**) A-FeOOH/$BiVO_4$ (8%).

The photocatalytic property over resultant photocatalysts was measured through producing O_2 from slitting water. Before producing O_2, to improve oxygen evolution rate, the sacrificial agent need be added. The previous report indicated that $BiVO_4$ could exhibit better photocatalytic performance for producing O_2 in the $NaIO_4$ solution than that in the $AgNO_3$ solution[48]. Meanwhile, to verify this result, we also measured the photocatalytic performance for producing O_2 over A-FeOOH/$BiVO_4$ photocatalyst in the same concentration $NaIO_4$ or $AgNO_3$ solution. As shown in Fig. S1, A-FeOOH/$BiVO_4$ photocatalyst in the $NaIO_4$ solution could present high oxygen evolution rate (OER) than A-FeOOH/$BiVO_4$ photocatalyst in the $AgNO_3$ solution. Hence, in this system, we selected $NaIO_4$ solution as the sacrificial agent. Then the results of oxygen evolution over all of photocatalysts were shown in Fig. 5A. For a series of resultant A-FeOOH/$BiVO_4$ photocatalysts, O_2 could be persistently produced with reaction time prolonging. Compared with pure $BiVO_4$, resultant A-FeOOH/$BiVO_4$ photocatalysts could clearly display the improvement of photocatalytic capacity for producing O_2. When loading amount

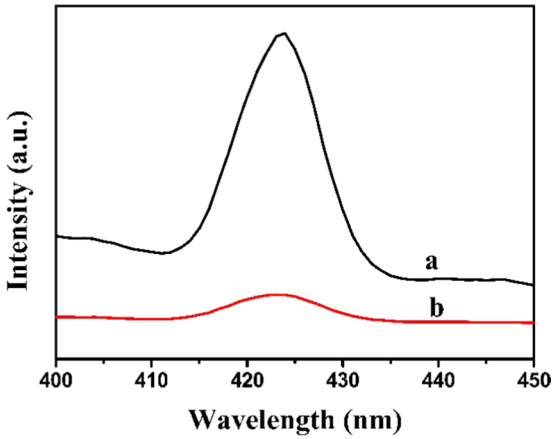

Figure 8. The photoluminescence spectra of (**a**) $BiVO_4$ and (**b**) A-FeOOH/$BiVO_4$ (8%).

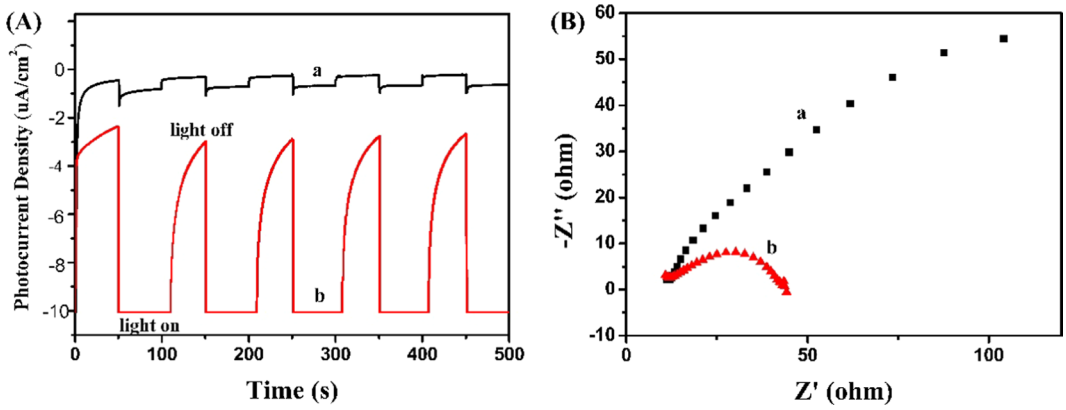

Figure 9. (**A**) Transient photocurrent property and (**B**) EIS of (a) $BiVO_4$ and (b) A-FeOOH/$BiVO_4$ (8%).

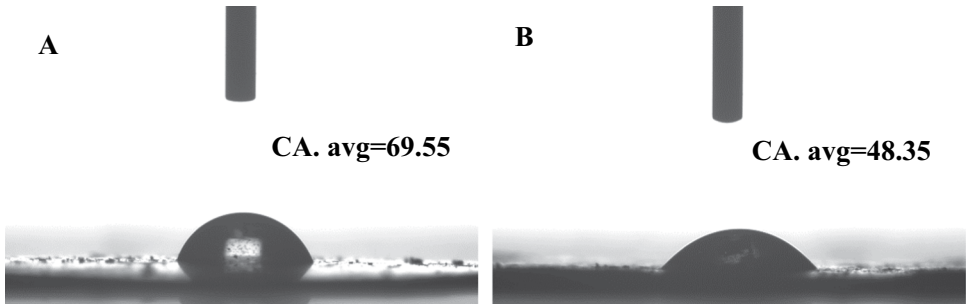

Figure 10. Water contact angle of (**A**) $BiVO_4$ and (**B**) A-FeOOH/$BiVO_4$(8 wt%).

of amorphous FeOOH was 8%, the sample had the optimal catalytic rate of O_2 evolution. Then Fig. 5B gives their OER. Their OER were 162.3, 691.7, 1077.1, 1206.3 and 962.8 μmol h^{-1} g^{-1} for pure $BiVO_4$, A-FeOOH/$BiVO_4$(2 wt%), A-FeOOH/$BiVO_4$(5 wt%), A-FeOOH/$BiVO_4$(8 wt%) and A-FeOOH/$BiVO_4$(10 wt%), respectively. The OER of A-FeOOH/$BiVO_4$(8 wt%) was around 7.4 folds more than pure $BiVO_4$. In addition, the O_2 production rates of different materials in previous reports have been in Table 1[49–52], and compared with this work. Obviously, as-prepared A-FeOOH/$BiVO_4$(8 wt%) in this work could present excellent advance.

Furthermore, as we known, the stability is a very significant index to appraise its ability. Thus, recycling tests for producing O_2 over A-FeOOH/$BiVO_4$(8 wt%) were investigated. As demonstrated in Fig. 6A, the A-FeOOH/$BiVO_4$(8 wt%) presented relative stable OER, after 6 times cycled experiments, as-prepared A-FeOOH/$BiVO_4$(8 wt%) still presented 70% photocatalytic activity of fresh sample. Besides, the XRD of used A-FeOOH/$BiVO_4$(8 wt%) was measured in Fig. 6B. Its XRD did not have obviously change in comparison to fresh A-FeOOH/

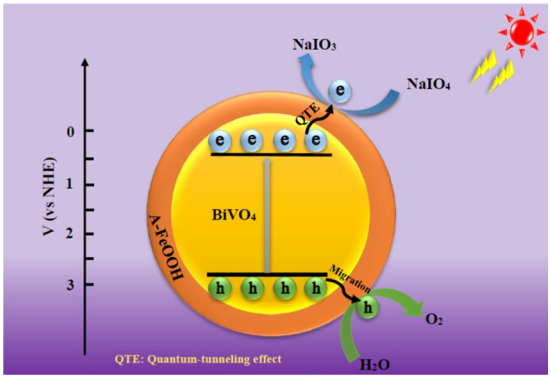

Figure 11. The proposed mechanism of photocatalytic water oxidation over A-FeOOH/$BiVO_4$ photocatalyst.

$BiVO_4$(8 wt%). And the morphology of used sample was also observed in Fig. 6C,D. It can be observed that used sample exhibited a certain aggregate in comparison to fresh sample, which might result in the declined photocatalytic property. Besides, the whole morphology did not present great change.

Obviously, it was found that covered amorphous FeOOH could effectively modify $BiVO_4$ to improve catalytic activity. Why? To find the reason for promoting effect, some analyzed instruments were tested to investigated light response capacity, the photoinduced charge separated rate and surface area of as-prepared photocatalysts, which are deemed as the main factors to effect on the photocatalytic performance[53–55].

Figure 7 presents the UV-Vis absorption spectrum of resulted $BiVO_4$ and A-FeOOH/$BiVO_4$(8 wt%). Pure $BiVO_4$ presented remarkable light absorption between 200 and 800 nm. The absorption edge was 525 nm. Band gap was 2.36 eV. After covered by amorphous FeOOH, the light absorption capacity of as-obtained A-FeOOH/$BiVO_4$(8 wt%) gained the obvious enhancement. Hence, the enhanced photocatalytic property might be anticipated.

Photoluminescence (PL) property could analyze the separation and transfer efficiency of photoinduced charges[56]. Therefore, the PL of $BiVO_4$ and A-FeOOH/$BiVO_4$ (8%) were measured in Fig. 8. The emission band intensity of A-FeOOH/$BiVO_4$ (8%) was clearly declined in comparison of pure $BiVO_4$. This result implied that covered amorphous FeOOH could effectively reduce the recombined efficiency of photoinduced electrons and holes, conducing to improve photocatalytic property[57].

Subsequently, electrochemistry measurements (photocurrent and EIS measurement) were used to assess the separated and transfer efficiency of photoinduced charges. Currently, the stronger photocurrent manifests the more effective separation and transfer rate of photo-charges[58,59]. As illustrated in Fig. 9A, pure $BiVO_4$ and A-FeOOH/$BiVO_4$(8 wt%) could produce certain intensity photocurrent signals. And the order of photocurrent intensity from strong to weak was A-FeOOH/$BiVO_4$(8 wt%) > pure $BiVO_4$. Evidently, resultant A-FeOOH/$BiVO_4$(8 wt%) exhibited the better photocurrent intensity, revealing that the separated rate of photogenerated charges for A-FeOOH/$BiVO_4$(8 wt%) photocatalyst was significantly improved by covering amorphous FeOOH.

Then EIS techniques were further used to estimate charge separation property. Figure 9B gives the EIS of pure $BiVO_4$ and A-FeOOH/$BiVO_4$(8 wt%). Small frequency semicircle radius exposes a better charge transfer rate. As demonstrated in Fig. 9B, the semicircle radius of A-FeOOH/$BiVO_4$(8 wt%) was shorter than that of pure $BiVO_4$, meaning that A-FeOOH/$BiVO_4$(8 wt%) possessed a higher separation and transport rate of photogenerated charges.

Besides, the BET surface area of pure $BiVO_4$ and A-FeOOH/$BiVO_4$(8 wt%) were 4.9 and 5.2 m^2g^{-1}, respectively. The addition of amorphous FeOOH had little effect on the surface area of photocatalyst. Additionally, the surface hydrophilic property of photocatalyst was performed to measure interact with the water. As presented in Fig. 10A,B, water contact angle (CA) of $BiVO_4$ (69.55°) and A-FeOOH/$BiVO_4$(8 wt%) (48.35°) was measured. This result meant that the covered amorphous FeOOH made $BiVO_4$ possess water favorable wetting capacity, providing a good chance to oxidate H_2O in aqueous environment[60].

Hence, combined with above analyzed results, it was found that, the main reason that as-prepare A-FeOOH/$BiVO_4$ possessed the better photocatalytic performance than $BiVO_4$ could be explained that the former exhibited higher efficiency for separation of photogenerated charges, and stronger strong visible responded activity compared with the latter. Hence, the remarkable improvement of photocatalytic capacity for producing O_2 was obtained.

Whereafter, to speculate the photocatalytic mechanism, the energy structure of $BiVO_4$ might be calculated[61]

$$Eg = E_{VB} - E_{CB} \quad (1)$$

$$E_{VB} = X - E_e + 1/2Eg \quad (2)$$

Herein Eg, E_{VB}, E_{CB}, X, E_e are band gap of photocatalyst, the valence band potential, conduction band potential, electro negativity of component atoms, hydrogen scale (4.5 eV), respectively. Here, for $BiVO_4$, X is 6.15 eV[62], Eg is 2.36 eV (Fig. 7). Hence, the CB and VB potentials of $BiVO_4$ were respective 0.47 and 2.83 eV.

Finally, in Fig. 11, a probable photocatalytic mechanism for A-FeOOH/$BiVO_4$ was presented. $BiVO_4$ could generate electrons and holes under light irradiation. Due to quantum-tunneling effect (QTE)[63,64], formed charges from the conduction band of $BiVO_4$ could transfer through amorphous FeOOH, or cationic vacancy network in amorphous FeOOH phase[65]. Then $NaIO_4$ as the electrons sacrificial agent consumed electrons. Because the cationic vacancy might be also activated by trapping hole[66], then holes remained on the VB of $BiVO_4$ would migrate to amorphous FeOOH surface to produce O_2. Hence, in this process, the existence of amorphous FeOOH could boost the separation of photoinduced charges for A-FeOOH/$BiVO_4$ system, obtaining the enhancement of photocatalytic performance.

Conclusions

We successfully produced a novel amorphous FeOOH modified $BiVO_4$, and investigated it photocatalytic performance for producing O_2 from water. It could be found that, amorphous FeOOH modified $BiVO_4$ exhibited higher migration rate of photogenerated charges, and strong visible responded capacity than $BiVO_4$, which resulted that amorphous FeOOH modified $BiVO_4$ could present better photocatalytic property than $BiVO_4$, and kept excellent performance and structure stability. Hence, this work provides a simple and inexpensive modified method for design and synthesis of effective photocatalysts.

Received: 21 September 2019; Accepted: 19 November 2019;
Published online: 13 December 2019

References

1. Li, X. *et al*. Engineering heterogeneous semiconductors for solar water splitting. *Journal of Materials Chemistry A* **3**, 2365–2534. (2015).
2. Zhu, Z., Kao, C. T., Tang, B. H., Chang, W. C. & Wu, R. J. Efficient hydrogen production by photocatalytic water-splitting using Pt-doped TiO_2 hollow spheres under visible light. *Ceramics International* **42**, 6749–6754 (2016).
3. Kisch, H. Semiconductor photocatalysis for chemoselective radical coupling reactions. *Accounts of Chemical Research* **50**, 1002–1010 (2017).
4. Wen, J. Q. *et al*. Photocatalysis fundamentals and surface modification of TiO_2 nanomaterials. *Chinese Journal of Catalysis* **36**, 2049–2070 (2015).
5. Huang, Z. A. *et al*. Effect of contact interface between TiO_2 and g-C_3N_4 on the photoreactivity of g-C_3N_4/TiO_2 photocatalyst: (001) vs (101) facets of TiO_2. *Applied Catalysis B: Environmental* **164**, 420–427 (2015).
6. Pan, D., Han, Z., Miao, Y., Zhang, D. & Li, G. Thermally stable TiO_2 quantum dots embedded in SiO_2 foams: Characterization and photocatalytic H_2 evolution activity. *Applied Catalysis B: Environmental* **229**, 130–138 (2018).
7. Pirhashemi, M., Habibi-Yangjeh, A. & Pouran, S. R. Review on the criteria anticipated for the fabrication of highly efficient ZnO-based visible-light-driven photocatalysts. *Journal of Industrial and Engineering Chemistry* **62**, 1–25 (2018).
8. Cui, L. F. *et al*. Facile preparation of Z-scheme WO_3/g-C_3N_4 composite photocatalyst with enhanced photocatalytic performance under visible light. *Applied Surface Science* **391**, 201–210. (2017).
9. Kumar, S. G. & Koteswara Rao, K. S. R. Comparison of modification strategies towards enhanced charge carrier separation and photocatalytic degradation activity of metal oxide semiconductors (TiO_2, WO_3 and ZnO). *Applied Surface Science* **391**, 124–148 (2017).
10. Li, L. *et al*. Nanotube array-like WO_3 photoanode with dual-Layer oxygen-Evolution cocatalysts for photoelectrocatalytic overall water splitting, ACS Applied Energy. *Materials* **1**, 6871–6880 (2018).
11. Chen, J. Z. *et al*. One-pot synthesis of CdS nanocrystals hybridized with single-layer transition-metal dichalcogenide nanosheets for efficient photocatalytic hydrogen evolution. *Angewandte Chemie International Edition* **54**, 1210–1214 (2014).
12. Wang, L. *et al*. Photosensitization of CdS by acid red-94 modified alginate: Dual ameliorative effect upon photocatalytic hydrogen evolution. *Applied Surface Science* **492**, 598–606 (2019).
13. Zhang, Y. C., Li, J., Zhang, M. & Dionysiou, D. D. Size-tunable hydrothermal synthesis of SnS_2 nanocrystals with high performance in visible light-driven photocatalytic reduction of aqueous Cr(VI). *Environmental Science & Technology* **45**, 9324–9331 (2001).
14. Hu, C., Lan, Y. Q., Qu, J. H., Hu, X. X. & Wang, A. M. Ag/AgBr/TiO_2 visible light photocatalyst for destruction of azodyes and bacteria. *Journal of Physical Chemistry B* **110**, 4066–4072 (2006).
15. Han, L., Wang, P., Zhu, C. Z., Zhai, Y. M. & Dong, S. J. Facile solvothermal synthesis of cube-like Ag@AgCl: a highly efficient visible light photocatalyst. *Nanoscale* **3**, 2931–2935 (2011).
16. Liu, R., Wang, P., Wang, X. F., Yu, H. G. & Yu, J. G. UV- and visible-light photocatalytic activity of simultaneously deposited and doped Ag/Ag(I)-TiO_2 photocatalyst. *Journal of Physical Chemistry C* **116**, 17721–17728 (2012).
17. Ai, Z. H., Huang, Y., Lee, S. C. & Zhang, L. Z. Monoclinic α-Bi_2O_3 photocatalyst for efficient removal of gaseous NO and HCHO under visible light irradiation. *Journal of Alloys and Compounds* **509**, 2044–2049 (2011).
18. Zhang, K. L., Liu, C. M., Huang, F. Q., Zheng, C. & Wang, W. D. Study of the electronic structure and photocatalytic activity of the BiOCl photocatalyst. *Applied Catalysis B: Environmental* **68**, 125–129 (2006).
19. Gao, M. C. *et al*. Surface decoration of BiOBr with $BiPO_4$ nanoparticles to build heterostructure photocatalysts with enhanced visible-light photocatalytic activity. *Separation and Purification Technology* **170**, 183–189 (2016).
20. Li, Y. Y., Wang, J. S., Yao, H. C., Dang, L. Y. & Li, Z. J. Efficient decomposition of organic compounds and reaction mechanism with BiOI photocatalyst under visible light irradiation. *Journal of Molecular Catalysis A:Chemical* **334**, 116–122 (2001).
21. Lin, F. *et al*. Low-cost dual cocatalysts $BiVO_4$ for highly efficient visible photocatalytic oxidation. *RSC Advances* **7**, 15053–15059 (2017).
22. Zhang, L., Chen, D. R. & Jiao, X. L. Monoclinic structured $BiVO_4$ nanosheets: hydrothermal preparation, formation mechanism, and coloristic and photocatalytic properties. *Journal of Physical Chemistry B* **110**, 2668–2673 (2006).
23. Zhou, S. *et al*. High-performance photoelectrochemical water splitting of $BiVO_4$@Co-MIm prepared by a facile *in-situ* deposition method. *Chemical Engineering Journal* **371**, 885–892 (2019).
24. Zhu, S. B., Xu, T. G., Fu, H. B., Zhao, J. C. & Zhu, Y. F. Synergetic effect of Bi_2WO_6 photocatalyst with C_{60} and enhanced photoactivity under visible irradiation. *Environmental Science &Technology* **41**, 6234–6239 (2007).
25. Zhang, L. W., Xu, T. G., Zhao, X. & Zhu, Y. F. Controllable synthesis of Bi_2MoO_6 and effect of morphology and variation in local structure on photocatalytic activities. *Applied Catalysis B: Environmental* **98**, 138–146 (2010).
26. Zhou, L. *et al*. A sonochemical route to visible-light-driven high-activity $BiVO_4$ photocatalyst. *Journal of Molecular Catalysis A: Chemical* **252**, 120–124 (2006).
27. Ke, D. N., Peng, T. Y., Ma, L., Cai, P. & Jiang, P. Photocatalytic water splitting for O_2 production under visible-light irradiation on $BiVO_4$ nanoparticles in different sacrificial reagent solutions, Applied. *Catalysis A: General* **350**, 111–117 (2008).
28. Sun, S. M., Wang, W. Z., Li, D. Z., Zhang, L. & Jiang, D. Solar light driven pure water splitting on quantum sized $BiVO_4$ without any cocatalyst, ACS. *Catalysis* **4**, 3498–3503 (2014).
29. Wang, Q. *et al*. Synthesis of MFe_2O_4 (M=Ni, Co)/$BiVO_4$ film for photoelectrochemical hydrogen production activity. *Applied Catalysis B: Environmental* **214**, 158–167 (2017).

30. Wang, X., Liao, D., Yu, H. & Yu, J. Highly efficient $BiVO_4$ single-crystal photocatalyst with selective Ag_2O-Ag modification: orientation transport, rapid interfacial transfer and catalytic reaction. *Dalton Transactions* **47**, 6370–6377 (2018).
31. Wang, Q. *et al*. $FeF_2/BiVO_4$ heterojuction photoelectrodes and evaluation of its photoelectrochemical performance for water splitting. *Chemical Engineering Journal* **337**, 506–514 (2018).
32. Cao, S. W. *et al*. Preparation of Au-$BiVO_4$ heterogeneous nanostructures as highly efficient visible-light photocatalysts. *ACS Applied Materials &Interfaces* **4**, 418–423 (2012).
33. Ge, L. Synthesis and characterization of novel visible-light-driven $Pd/BiVO_4$ composite photocatalysts. *Materials Letters* **62**, 926–928 (2008).
34. Zhang, J. *et al*. Novel AuPd bimetallic alloy decorated 2D $BiVO_4$ nanosheets with enhanced photocatalytic performance under visible light irradiation. *Applied Catalysis B: Environmental* **204**, 385–393 (2017).
35. Zhang, K. *et al*. Co–$Pd/BiVO_4$: High-performance photocatalysts for the degradation of phenol under visible light irradiation. *Applied Catalysis B: Environmental* **224**, 350–359 (2018).
36. Lin, Z., Du, C., Yan, B., Wang, C. & Yang, G. Two-dimensional amorphous NiO as a plasmonic photocatalyst for solar H_2 evolution. *Nature Communications* **9**, 4036 (2018).
37. Kang, Y. *et al*. An amorphous carbon nitride photocatalyst with greatly extended visible-light-responsive range for photocatalytic hydrogen generation. *Advanced Materials* **27**, 4572–4577 (2015).
38. Chowdhury, M., Ntiribinyange, M., Nyamayaro, K. & Fester, V. Photocatalytic activities of ultra-small β-FeOOH and TiO_2 heterojunction structure under simulated solar irradiation. *Materials Research Bulletin* **68**, 133–141 (2015).
39. Zheng, Y., Zhang, Z. S. & Li, C. H. Beta-FeOOH-supported graphitic carbon nitride as an efficient visible light photocatalyst. *Journal of Molecular Catalysis A: Chemical.* **68**, 133–141 (2015).
40. Sun, M., Senthil, R. A., Pan, J., Osman, S. & Khan, A. A facile synthesis of visible-light driven rod-on-rod like α-FeOOH/α-$AgVO_3$ nanocomposite as greatly enhanced photocatalyst for degradation of rhodamine B. *Catalysts* **8**, 392 (2018).
41. Chemelewski, W. D., Lee, H. C., Lin, J. F., Bard, A. J. & Mullins, C. B. Amorphous FeOOH oxygen evolution reaction catalyst for photoelectrochemical water splitting. *Journal of the American Chemical Society* **136**, 2843–2850 (2014).
42. Liu, J., Zheng, M., Shi, X., Zeng, H. & Xia, H. Amorphous FeOOH quantum dots assembled mesoporous film anchored on grapheme nanosheets with superior electrochemical performance for supercapacitors. *Advanced Functional Materials* **26**, 919–930 (2016).
43. Xu, H. *et al*. Synthesis, characterization and photocatalytic activities of rare earth-loaded $BiVO_4$ catalysts. *Applied Surface Science* **256**, 597–602 (2009).
44. Zhang, B. B., Wang, L., Zhang, Y. J., Ding, Y. & Bi, Y. P. Ultrathin FeOOH nanolayers with abundant oxygen vacancies on $BiVO_4$ photoanodes for efficient water oxidation. *Angewandte Chemie International Edition* **57**, 2248–2252 (2018).
45. Xu, D. *et al*. MOF-derived Co_3O_4 thin film decorated $BiVO_4$ for enhancement of photoelectrochemical water splitting. *Applied Surface Science* **491**, 497–504 (2019).
46. Chen, R. *et al*. $BiVO_4/\alpha$-Fe_2O_3 catalytic degradation of gaseous benzene: preparation, characterization and photocatalytic properties. *Applied Surface Science* **427**, 141–147 (2018).
47. Huang, J., Ding, Y., Luo, X. & Feng, Y. Solvation effect promoted formation of p–n junction between WO_3 and FeOOH: A high performance photoanode for water oxidation. *Journal of Catalysis* **333**, 200–206 (2016).
48. Wang, J. & Osterloh, F. E. Limiting factors for photochemical charge separation in $BiVO_4/Co_3O_4$, a highly active photocatalyst for water oxidation in sunlight. *Journal of Materials Chemistry A* **2**, 9405–9411 (2014).
49. Xin, G., Guo, W. & Ma, T. Effect of annealing temperature on the photocatalytic activity of WO_3 for O_2 evolution. *Applied Surface Science* **256**, 165–169 (2009).
50. Wang, Z. *et al*. $BiVO_4$ nano–leaves: Mild synthesis and improved photocatalytic activity for O_2 production under visible light irradiation. *CrystEngComm* **13**, 2500–2504 (2011).
51. Kudo, A., Ueda, K., Kato, H. & Mikami, I. Photocatalytic O_2 evolution under visible light irradiation on $BiVO_4$ in aqueous $AgNO_3$ solution. *Catalysis Letters* **53**, 229–230 (1998).
52. Zhu, J. *et al*. Hierarchical hollow spheres composed of ultrathin Fe_2O_3 nanosheets for lithium storage and photocatalytic water oxidation. *Energy & Environmental Science* **6**, 987–993 (2013).
53. Ananpattarachai, J., Kajitvichyanukul, P. & Seraphin, S. Visible light absorption ability and photocatalytic oxidation activity of various interstitial N-doped TiO_2 prepared from different nitrogen dopants. *Journal of Hazardous Materials* **168**, 253–261 (2009).
54. Liao, G. Z., Chen, S., Quan, X., Yu, H. T. & Zhao, H. M. Graphene oxide modified g-C_3N_4 hybrid with enhanced photocatalytic capability under visible light irradiation. *Journal of Materials Chemistry* **22**, 2721–2726 (2012).
55. Liu, B. *et al*. Doping high-surface-area mesoporous TiO_2 microspheres with carbonate for visible light hydrogen production. *Energy & Environmental Science* **7**, 2592–2597 (2014).
56. Humayun, M. *et al*. Enhanced visible-light activities of porous $BiFeO_3$ by coupling with nanocrystalline TiO_2 and mechanism. *Applied Catalysis B: Environmental* **180**, 219–226 (2016).
57. Guo, Y., Ao, Y., Wang, P. & Wang, C. Mediator-free direct dual-Z-scheme $Bi_2S_3/BiVO_4/MgIn_2S_4$ composite photocatalysts with enhanced visible-light-driven performance towards carbamazepine degradation. *Applied Catalysis B: Environmental* **254**, 479–490 (2019).
58. Lv, D. *et al*. One-pot combustion synthesis of $BiVO_4$/BiOCl composites with enhanced visible-light photocatalytic properties. *Separation and Purification Technology* **174**, 97–103 (2017).
59. Shi, L., Ma, J., Yao, L., Cui, L. & Qi, W. Enhanced photocatalytic activity of $Bi_{12}O_{17}Cl_2$ nano-sheets via surface modification of carbon nanotubes as electron carriers. *Journal of Colloid and Interface Science* **519**, 1–10 (2018).
60. Fan, Y. *et al*. Three-dimensional branched crystal carbon nitride with enhanced intrinsic peroxidase-like activity: A hypersensitive platform for colorimetric detection. *ACS Applied Materials &Interfaces* **11**, 17467–17474 (2019).
61. Kumar, A. *et al*. Facile hetero-assembly of superparamagnetic Fe3O4/BiVO4 stacked on biochar for solar photo-degradation of methyl paraben and pesticide removal from soil. *Journal of Photochemistry and Photobiology A: Chemistry* **337**, 118–131 (2017).
62. Selvarajan, S., Suganthi, A., Rajarajan, M. & Arunprasath, K. Highly efficient $BiVO_4/WO_3$ nanocomposite towards superior photocatalytic performance. *Powder Technology* **307**, 203–212 (2017).
63. Yu, Z. *et al*. Noninvasively modifying band structures of wide-band gap metal oxides to boost photocatalytic activity. *Advanced Materials* **30**, 1706259 (2018).
64. Huang, L. *et al*. Dual cocatalysts loaded type I CdS/ZnS core/shell nanocrystals as effective and stable photocatalysts for H_2 evolution. *Journal of Physical Chemistry C* **117**, 11584–11591 (2013).
65. Richters, J.-P., Voss, T., Kim, D. S., Scholz, R. & Zacharias, M. Enhanced surface-excitonic emission in ZnO/Al_2O_3 core–shell nanowires. *Nanotechnology* **19**, 305202 (2008).
66. Ning, X., Zhen, W., Wu, Y. & Lu, G. Inhibition of CdS photocorrosion by Al_2O_3 shell for highly stable photocatalytic overall water splitting under visible light irradiation. *Applied Catalysis B: Environmental* **226**, 373–383 (2018).

Acknowledgements

This work was supported by National Natural Science Foundation of China (21671092, 21401093), LiaoNing Revitalization Talents Program (XLYC1802057), basic research projects of Liaoning Provincial Education Department (L2017LQN004, L2017LQN006) and talent scientific research fund of LSHU (No. 2016XJJ-080).

Author contributions

Ying Zhang prepared photocatalysts and measured performance. Lei Shi wrote the main manuscript text. Zhongxing Geng and Tieqiang Ren measured the chemical structure of catalyst. Zhanxu Yang designed catalyst.

Competing interests

The authors declare no competing interests.

Additional information

Supplementary information is available for this paper at https://doi.org/10.1038/s41598-019-54940-2.

Correspondence and requests for materials should be addressed to L.S. or Z.Y.

Reprints and permissions information is available at www.nature.com/reprints.

Publisher's note Springer Nature remains neutral with regard to jurisdictional claims in published maps and institutional affiliations.